The Astronomical Journal, 127:489–500, 2004 January

PERIODICITIES IN THE X-RAY INTENSITY VARIATIONS OF TV COLUMBAE: AN INTERMEDIATE POLAR

V. R. Rana[1] and K. P. Singh
Department of Astronomy and Astrophysics, Tata Institute of Fundamental Research, Homi Bhabha Road, Mumbai 400 005, India; vrana@tifr.res.in, singh@tifr.res.in

E. M. Schlegel
Harvard-Smithsonian Center for Astrophysics, 60 Garden Street, Cambridge, MA 02138; ems@head-cfa.harvard.edu

and

P. Barrett
ESS/Science Software Group, Space Telescope Science Institute, 3700 San Martin Drive, Baltimore, MD 21218; barrett@stsci.edu
Received 2003 August 12; accepted 2003 September 26

ABSTRACT

We present results from a temporal analysis of the longest and the most sensitive X-ray observations of TV Columbae—a cataclysmic variable classified as an intermediate polar. The observations were carried out with the *Rossi X-Ray Timing Explorer* (*RXTE*) Proportional Counter Array, *ROSAT* Position Sensitive Proportional Counter, and *ASCA*. Data were analyzed using a one-dimensional CLEAN and Bayesian algorithms. The presence of a nearly sinusoidal modulation due to the spin of the white dwarf is seen clearly in all the data, confirming the previous reports based on the *EXOSAT* data. An improved period of 1909.7 ± 2.5 s is derived for the spin from the *RXTE* data. The binary period of 5.5 hr is detected unambiguously in X-rays for the first time. Several sidebands due to the interaction of these periods are observed in the power spectra, thereby suggesting contributions from both the disk-fed and the stream-fed accretion for TV Col. The accretion disk could perhaps be precessing, as sidebands due to the influence of 4 day period on the orbital period are seen. The presence of a significant power at certain sidebands of the spin frequency indicates that the emission poles are asymmetrically located. The strong power at the orbital sidebands seen in both the *RXTE* and *ROSAT* data gives an indication for an absorption site fixed in the orbital frame. Both the spin and the binary modulation are found to be energy dependent. The fact that the spin modulation amplitude in TV Col decreases with energy is confirmed. Hardness ratio variations and the energy-dependent modulation depth during the spin modulation can be explained by partially covered absorbers in the path of the X-ray emission region in the accretion stream. Increased hardness ratio during a broad dip in the intensity at binary phase of 0.75–1.0 confirms the presence of a strong attenuation due to additional absorbers, probably from an impact site of the accretion stream with the disk or magnetosphere.

Key words: accretion, accretion disks — binaries: close — novae, cataclysmic variables — stars: individual (TV Columbae) — X-rays: stars

1. INTRODUCTION

The cataclysmic variable (CV) TV Columbae is classified as an intermediate polar (IP) containing a magnetic white dwarf accreting from the Roche lobe of a late-type dwarf companion via an accretion disk and an accretion channel. It was identified by Charles et al. (1979) as the optical counterpart of a hard X-ray source (2A 0526-328) first discovered with the *Ariel 5* satellite (Cooke et al. 1978). An optical star with $V \sim 13$–14 mag, TV Col is at a distance of 368^{+17}_{-15} pc (McArthur et al. 2001).

A 1911 ± 5 s period has been detected from this source in X-rays using the *EXOSAT* observatory (Schrijver, Brinkman, & van der Woerd 1987). The X-ray period has been identified as the spin period of the white dwarf, and the spin-phased light curves have been found to be energy dependent (Norton & Watson 1989). X-ray observations of TV Col have also been reported from the *ROSAT*, *ASCA*, and *Ginga* satellites by Vrtilek et al. (1996), Ezuka & Ishida (1999), and Ishida & Fujimoto (1995), respectively, but they mainly discuss the spectral characteristics of the source rather than the timing properties. Vrtilek et al. (1996), however, reported a failure to detect the X-ray spin period in the *ROSAT* observation analyzed by them. A period of 1938 ± 10 s was claimed to be present in the optical bands (*UBV*) at a level of $\sim$6% (full amplitude) by Bonnet-Bidaud, Motch, & Mouchet (1985; see their note added in proof) after the discovery of 32 minute period in X-rays with the *EXOSAT* satellite was reported by Schrijver et al. (1985).

TV Col also exhibits additional periods of 5.2 hr, 5.5 hr, and 4 days (Motch 1981; Hutchings et al. 1981; Bonnet-Bidaud et al. 1985; Barrett, O'Donoghue, & Warner 1988; Hellier, Mason, & Mittaz 1991; Hellier 1993; Augusteijn et al. 1994) observed in optical photometry and spectroscopy, which add further complexities. None of these periods have been seen convincingly in the X-ray observations reported so far, although Hellier, Garlick, & Mason (1993) did report some evidence for intensity dips separated by an orbital cycle in the data taken with the *EXOSAT* observatory. The spectroscopic period of 5.5 hr is believed to represent the binary orbital modulation and shows partial eclipses. The 4 day period is possibly due to the nodal precession of the accretion disk around the white dwarf (Barrett et al. 1988; Hellier 1993). The 4 day period was also reported from UV observations by

[1] Joint Astronomy Programme, Department of Physics, Indian Institute of Science, Bangalore 560 012, India.

Mateo, Szkody, & Hutchings (1985). The 5.2 hr period likely represents the beat between the 5.5 hr and 4 day periods. Recently Retter et al. (2003) have reported another period at 6.3 hr in the optical data and identified it as representing the permanent positive superhump period of the binary system. The positive superhump is usually explained as the beat between the binary period and the precession of an eccentric accretion disk in the apsidal plane (see reviews by Patterson 2001; O'Donoghue 2000).

The power spectrum of IPs in X-ray band can be very complex containing the fundamental system frequencies, their harmonics, and sometimes the sideband frequencies due to beating of the fundamental periods and their harmonics. The X-rays, which are believed to originate from the shock-heated plasma region near the surface of the white dwarf, show modulation at all or some of the above-mentioned frequency components. Hence a long and well-sampled hard X-ray data particularly taken from an instrument with large effective area and high time resolution can provide important clues about the mode of accretion and the geometry of these sources.

Here, we report on the longest and the most sensitive broadband X-ray observations carried out in the hard X-rays with the *Rossi X-Ray Timing Explorer* (*RXTE*) and in the soft X-rays with the *ROSAT* satellites. Although these observations are not simultaneous these are the best available for carrying out temporal analysis to search for various periodicities in the X-ray emission from TV Col and to study their energy dependence. Results from the timing analysis of simultaneous soft and hard X-ray observations with the *ASCA* satellite are also presented. A detailed timing analysis of these observations has not been reported so far except for a preliminary report in Singh et al. (2003). The paper is organized as follows: In the next section, we present details of observations and data reduction in the hard X-ray and the soft X-ray energy bands. Section 3 contains results obtained from the power spectral analysis and the light curves folded on the spin period and the orbital period of the system, followed by a discussion and interpretation of results in § 4. Finally, we present a summary of our results and the conclusions in § 5.

2. OBSERVATIONS AND DATA REDUCTION

2.1. *Hard X-Rays*

TV Col was observed with the Proportional Counter Array (PCA) on board the *RXTE* during the years 1996 (PI: E. Schlegel) and 2000 (PI: K. Mukai). The PCA consists of five Proportional Counter Units (PCUs), each filled with xenon gas and split into three layers, plus a propane filled veto layer. Each PCU has a large collecting area of 1300 cm^2, energy bandwidth of 2–60 keV and a collimator with a field of view of 1° (FWHM). The energy resolution of a PCU is $\sim$18% at 6 keV. More details about the PCA can be found in Jahoda et al. (1996).

The complete observation log is given in Table 1. Columns (1) and (2) list the start and end times of the observation. The name of the satellite is given in column (3), and the effective exposure times are given in column (4). The mean source count rates in 2–20 keV energy band for the *RXTE*, 0.1–2.2 keV energy band for the *ROSAT*, and 0.7–10 keV energy band for the *ASCA*, after background subtraction (see below), are given in column (5), followed by comments on the frequency and duration of each exposure in column (6). All the PCUs were "ON" during most of the 1996 observations, whereas only three PCUs were "ON" during the 2000 observations. Of the total exposure time of 79 ks in 1996, the time for which less than five PCUs were "ON" was $\sim$12 ks. The count rates shown are scaled to the same number of PCUs assuming identical area for each PCU.

TABLE 1

Summary of the *ROSAT*, *RXTE*, and *ASCA* Observations of TV Columbae

Start Time (UT) (1)	End Time (UT) (2)	Satellite (3)	Exposure (ks) (4)	Mean Count[a,b] rate (count s^{-1}) (5)	Comments (6)
1991 Feb 18, 0805.....	Feb 20, 1530	*ROSAT*	8.6	0.43	Four exposures over 2 days, each for $\sim$2 ks
1992 Sep 28, 0413.....	Sep 30, 1551	*ROSAT*	5.7	0.39	Three exposures widely separated over 2 days, each for $\sim$2 ks
1993 Feb 9, 2009.....	Feb 11, 0614	*ROSAT*	22.6	0.43	14 exposures over 2 days, each for $\sim$2 ks
1996 Aug 9, 1422.....	Aug 13, 2012	*RXTE*	79	32.4	Six to eight exposure per day, each for 2 to 3.6 ks for a 4.2 day long observation
2000 Dec 7, 0728.....	Dec 9, 1229	*RXTE*	22	33.0	Two to four exposures per day, each for 2 to 3.6 ks for more than 2 day long observations
1995 Feb 28, 0808.....	Feb 1, 1040	*ASCA*	24.7	0.58	26 exposures over $\sim$1 day, each for less than 2 ks

[a] The 0.1–2.2 keV energy band for the *ROSAT*, 2–20 keV energy band for the *RXTE* and 0.7–10 keV energy band for the *ASCA* satellite.
[b] *RXTE* count rates have been normalized for 5 PCUs (see the text).

The PCA data were processed using the standard programs of the software package FTOOLS 5.1.[2] Both standard 1 (time resolution of 1 s) and standard 2 (time resolution of 16 s) data were extracted and analyzed.

X-ray light curves (source plus background) were obtained using the following selection criteria: we use only the "good time interval" (GTI) data when extracting the light curves using the SAEXTRCT program in FTOOLS. The GTI selects data when the Earth elevation angle is greater than 10° and the offset between the pointing direction of the satellite and the centre of the field of view is less than $0\overset{\circ}{.}02$. The times of high concentration of electrons that increase the noise at low energies were excluded. The latest set of combined background models "CM L7 Linear" for faint sources were used to create the background light curves for each observation. The background light curves were then subtracted from the (source plus background) light curves to produce the X-ray light curves for the source.

We analyzed the standard 2 data from only the top xenon layer of the PCA for a better signal-to-noise ratio than is obtainable from the three layers combined. Light curves in the energy band of 2–20 keV were thus extracted and analyzed. The mean normalized count rate was found to be nearly the same in the 1996 and the 2000 observations (see Table 1). The normalized X-ray light curve in the 2–20 keV energy band with a bin time of 64 s is shown in Figure 1 for the 1996 observations. The observations done in the year 2000 suffered from poor sampling (see Table 1), and are therefore not analyzed any further.

2.2. *Soft X-Rays*

TV Col was observed thrice with the *ROSAT* (Trümper 1983) Position Sensitive Proportional Counter (PSPC) during 1991–1993 (PI: S. D. Vrtilek for 1991 observation and P. Barrett for 1992 and 1993 observations). The observation log is given in Table 1. The X-ray image and the light curves were extracted using the XSELECT program in the FTOOLS. The soft X-ray light curve of TV Col was obtained by extracting the counts with a resolution of 4 s from the unsmoothed PSPC images using a circle with a radius of $3\overset{\prime}{.}75$ centered on the peak position. The background was estimated from several neighboring source-free regions and found to be steady with a count rate of 0.041 counts s^{-1}. The observed count rate, after background subtraction, varies between 0.2 and 0.7 counts s^{-1} during each of the three observations. There are no confusing sources in the neighborhood, the next brightest source in the vicinity is about 10 times fainter and $10\overset{\prime}{.}5$ away. We have performed a detailed analysis of the X-ray data from the longest observation with an exposure time of 22,557 s obtained during 1993 February 9–11. The source X-ray light curve in the 0.1–2.2 keV energy band with a bin time of 128 s is shown in Figure 2 for the 1993 observation. The two observations in 1991 and 1992 were very short and infrequent (see Table 1) and are therefore not analyzed any further. Analysis of the 1991 observation was presented by Vrtilek et al. (1996).

In addition to the analysis of the above soft and hard X-ray data separated by 3 yr, we have also analyzed a simultaneously obtained 0.7–10 keV data from the *ASCA* SIS0 (Yamashita et al. 1997) observations during 1995 February 28 to March 1. (See Table 1 for details). We analyzed SIS0 "bright2" mode data with a time resolution of 16 s. We applied a strict screening

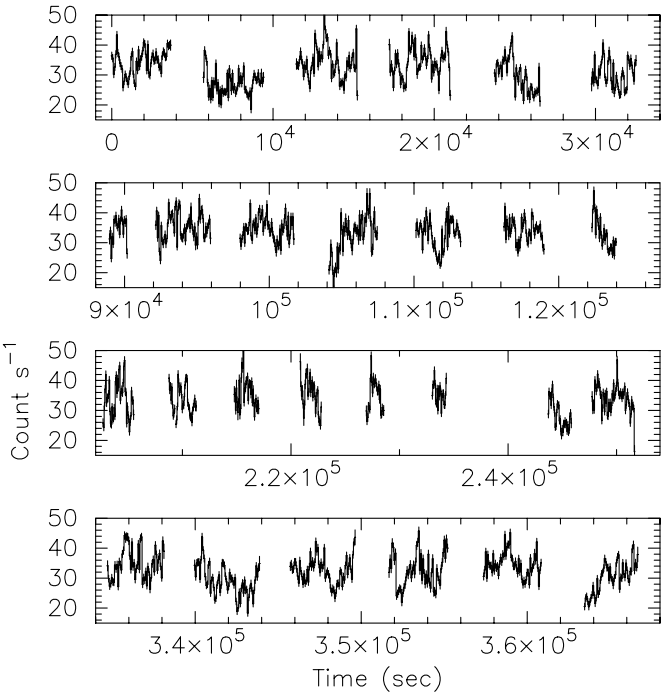

FIG. 1.—Light curve of TV Col in the 2–20 keV energy band obtained with *RXTE* during 1996 August 9–13. The bin time is 64 s for the four panels. Time zero corresponds to TJD 10,304.5985.

criteria for the parameter "RBM-CONT" setting its value less than 75 instead of the standard screening. This essentially removes the excess count rate due to a flare mainly in the soft X-rays (below 2 keV). Source photons were extracted from a circular region with a radius of $4'$ centered on the peak position. The background light curves were extracted from the neighboring CCD chip, which is free from the source counts.

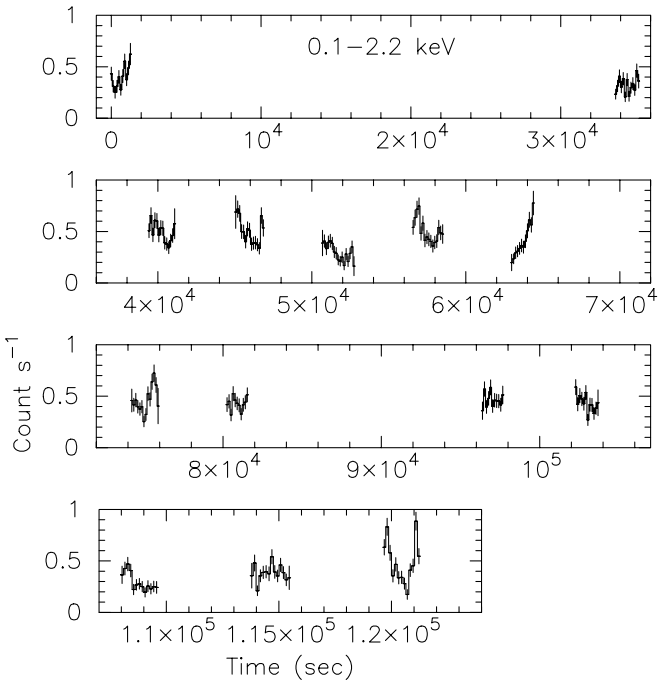

FIG. 2.—Light curve of TV Col in the 0.1–2.2 keV energy band obtained with *ROSAT* during 1993 February 9–11. The bin time is 128 s for the four panels. Time zero corresponds to TJD 9,027.2597.

[2] The information about FTOOLS can be found at http://heasarc.gsfc.nasa.gov/docs/corp/software.html.

The observed count rate, after the background subtraction, varies between 0.3 and 0.9 counts s^{-1} with an average value of $\sim$0.6 counts s^{-1}. The spectra corresponding to the source and the background were also extracted from the corresponding regions. Results from a detailed spectral analysis of these data were reported by Ezuka & Ishida (1999).

In this paper, we will mainly concentrate on the analysis of the *RXTE* and the *ROSAT* data, using the *ASCA* data only to verify some of the results.

3. ANALYSIS AND RESULTS

3.1. *Power Spectra*

Of the six observations listed in Table 1, only three observations, namely the 1993 (*ROSAT*), the 1996 (*RXTE*), and the 1995 (*ASCA*), are sufficiently long and with good sampling (i.e., more exposure and less gap between them) to provide adequate frequency resolution to search for the fundamental periods, their harmonics, and sideband components in the power spectral distribution of the X-ray light curves of TV Col. The frequency resolution is best for the 1996 *RXTE* data with a value of 6.8184×10^{-7} s^{-1}. The 1993 *ROSAT* data and the 1995 *ASCA* data have frequency resolutions of 2.0605×10^{-6} s^{-1} and 2.6179×10^{-6} s^{-1}, respectively. All observations from the *ROSAT*, the *RXTE*, and the *ASCA* satellites have gaps due to occultation of the source by the Earth and the times when the instruments are switched off during the passage of the satellites through regions of high particle background like South Atlantic Anomaly. This leads to complications in the power spectrum as the true variations in the source are further modulated by the irregular and infrequent sampling defined by the window function of the data. Therefore, the "dirty" power density spectrum first calculated from the light curve was followed by the deconvolution of the "window" function from the data using the one-dimensional "CLEAN" algorithm as implemented in the PERIOD program (Version 5.1) available in the STARLINK package (see Roberts, Lehar, & Dreher 1987 for details on the CLEAN method). We applied the barycentric correction to all the data sets before carrying out the power spectral analysis.

The dirty power spectrum obtained from the 1996 *RXTE* observation in the 2–20 keV energy band is shown in Figure 3 (*top*). The corresponding window power spectrum is shown plotted in the middle panel. The CLEANed power spectrum after deconvolution of the window power is presented in the bottom panel of the figure. The power plotted (here and below) is square of half the amplitude of the corresponding sinusoidal component at that frequency. Similarly, the CLEANed power spectrum obtained from the 1993 *ROSAT* observation in the energy band of 0.1–2.2 keV is shown in Figure 4 along with its dirty power and the window power. The CLEANed power spectra presented here were obtained after 1000 iterations of the CLEAN procedure with a loop gain of 0.1. A large value of CLEAN iterations with a small value of loop gain result in a stable power spectrum with significant noise reduction (Norton et al. 1992a, 1992b). Excessive cleaning can, however, result in a considerable reduction of the amplitude of the real peak. We chose the optimum values of the above two parameters such that the reduction in the amplitude of real peak is minimum and the reduction in the noise is maximum. Since we could get the direct measurement of amplitude from the spin-folded light curves, we used it as a control for deciding the number of iterations and gain values. After 1000 iterations, the amplitude of the peak corresponding to the spin period of the system

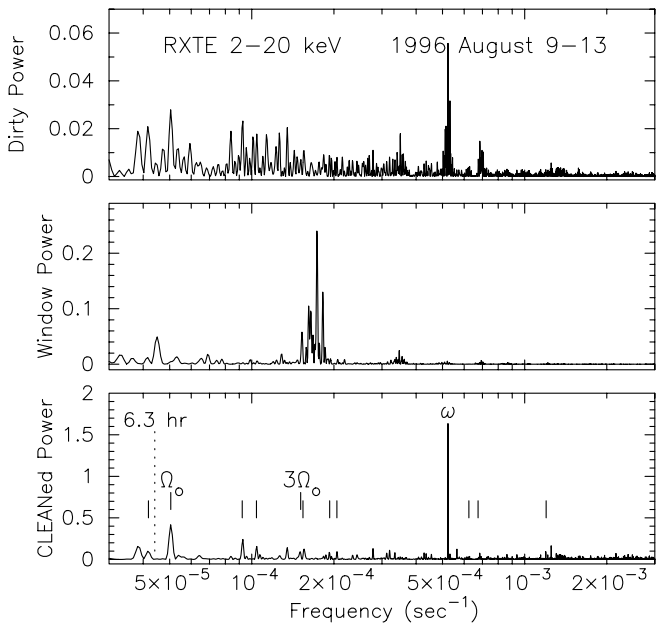

FIG. 3.—Power spectra of TV Col in the 2–20 keV energy band from the 1996 *RXTE* observations. *Top*: a dirty power spectrum; *middle*, its corresponding window power. *Bottom*: a CLEANed power spectrum for TV Col. The tick marks show locations of various components that are detected and identified with components relevant to TV Col at frequencies corresponding to the spin period (ω), orbital period (Ω_0), their sidebands, and also the sideband frequencies with precession period (Ω_{pr}) (see Table 2). The location of 6.3 hr superhump period (Retter et al. 2003) is marked with a vertical dotted line.

reduced by only $\sim$15% (typical in such applications, e.g., Norton, Beardmore, & Taylor 1996). Several peaks can be seen in the power spectra shown in Figures 3 and 4. Peaks seen in a power spectrum can correspond both to actual frequencies of the system and to the noise present in the data. In order to

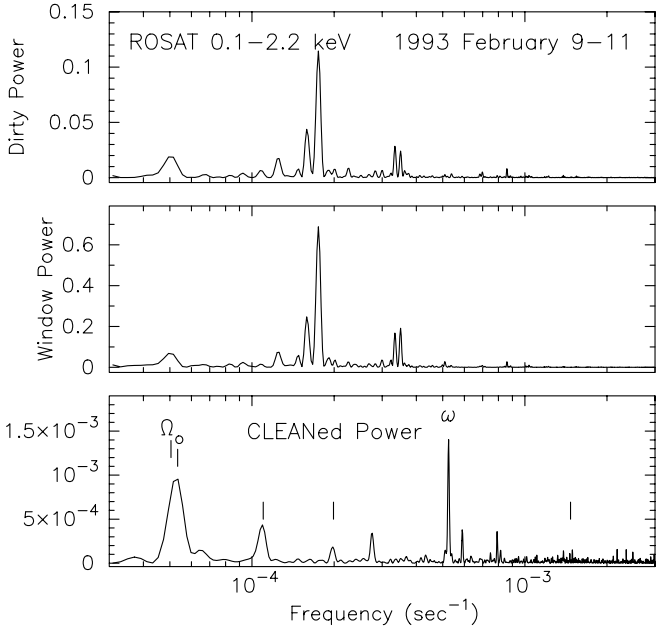

FIG. 4.—Same as in Fig. 3, but for the 1993 *ROSAT* observations in 0.1–2.2 keV energy band. Due to the poorer sampling and shorter length of observation, the peaks are not as well resolved here as in the *RXTE* data. See Table 2 for the corresponding tick mark frequency components.

determine which of the peaks are because of the system, we had to estimate the noise level in the power spectra. To estimate the noise level, a procedure similar to the one described in Norton et al. (1996) was followed. The absolute amplitude of the power level above which at least $N/10$ number of noise peaks are present, where N is the number of independent frequency samples, was estimated. The value of N can vary according to the length of observation and the time resolution of the light curve from which the power spectrum has been obtained. This estimated value of noise level corresponds to 90% confidence limit, since there is only 10% chance that the peak above this level is due to noise. The noise level determined this way is given in Table 2, and the peaks above this level are considered to be real. The noise in the CLEANed power spectra estimated this way is nearly constant in the frequency range of interest.

In order to further confirm whether the peaks present in the CLEANed power spectra above the noise level are indeed related to the system, an independent method namely the ''Bayesian'' method was adopted. This method is particularly useful for the detection of a periodic signal in the data when there is no prior knowledge about the presence of such a signal or its characteristics. It is also equally sensitive to sinusoidal and nonsinusoidal modulations, since it does not require a prior information about the shape of the signal. This approach is mathematically more rigorous and can provide an optimum number of frequencies allowed by data with a better accuracy. Detailed information about this method can be found in Bretthorst (1988), and the comparison of this method with the other more commonly used methods like Fast Fourier Transform and epoch folding is presented in Gregory & Loredo (1996). The Bayesian method is an iterative method in which a periodogram of the log of Student t-distribution versus frequencies is generated. Student t-distribution is essentially a posterior probability density that a frequency ω is present in the data, when no prior information about it is available. The dominant period corresponding to the highest probability is then identified in the periodogram and made as a part of the model by specifying its period. This essentially removes that period from the light curve. This procedure is repeated for the other dominant periods in the periodogram. The periodogram obtained using this algorithm also showed two dominant peaks corresponding to the spin period and the orbital period of the system, apart from other frequency components. Several peaks present in the CLEANed power spectrum were thus identified using the Bayesian algorithm. This list of identified components for TV Col was then compared with the list of expected components (Table 1 of Norton et al. 1996). The absolute power corresponding to various identified system components are listed in Table 2. In order to match the observed frequency components with the expected components, we calculated a 90% confidence interval, for each of the observed peak centroid by fitting a Gaussian model. If the expected component is within this 90% confidence interval, we considered it to be a match. Apart from these identified components, there are several other unidentified peaks with power well above the noise level but do not match with any of the system frequency. In Table 2, we have listed the frequency components that are identified with the system components and are confirmed using the Bayesian method. Strong but unidentified peaks are also listed in Table 2. Of these, about 65% were confirmed using the Bayesian method. Only the identified frequency components are marked in Figures 3 and 4. In the rest of the paper, however, we will discuss the power spectra obtained using the CLEAN method but focus only on the frequencies confirmed using the Bayesian method.

The power spectra shown in Figures 3 and 4 show a dominant peak at a frequency, ω, corresponding to a period of 1909.7 ± 2.5 s derived from the 1996 *RXTE* data and 1903.3 ± 7.5 s from the 1993 *ROSAT* data. The strength of the peak at these periods suggests that ω is very likely to be the spin frequency of the white dwarf in TV Col. The errors on these periods are derived by calculating the half-bin size of a single frequency bin, centered on the peak present in the periodogram. These values are consistent with the previously reported value of 1911 ± 5 s (Schrijver et al. 1987; Norton & Watson 1989) from the *EXOSAT* data. Significant power is also observed at periods corresponding to a value of 19819 ± 267 s from the 1996 *RXTE* and 19413 ± 770 s from the 1993 *ROSAT* data, consistent with the 5.5 hr (19,800 s) orbital period (the corresponding orbital frequency is represented here by Ω_0). This period is detected without any ambiguity in *RXTE* data but is merged with other nearby components in the *ROSAT* data. Since both the data sets show the presence of Ω_0 component, a strong orbital modulation is expected to be present in the data. Several sideband frequencies due to interactions among these periods are also seen. Power at the sideband frequencies $\omega + \Omega_0$, $\omega + 2\Omega_0$, $\omega + 3\Omega_0$, $2\omega + 3\Omega_0$, and $3\omega - 2\Omega_0$ are seen above the noise. A modulation at the sidebands due to the interaction of the orbital and the 4 day period due to the precession of disk (precession frequency, $\Omega_{\rm pr}$) is also observed. The value adopted for the precession frequency is 2.8935×10^{-6} s^{-1} (Barrett et al. 1988; Hellier 1993). Power seen at a frequency component corresponding to the 5.2 hr period is identified with the sideband frequency corresponding to $\Omega_0 + \Omega_{\rm pr}$ in the *RXTE* data (in 2–5 keV energy band) but is not resolvable in the *ROSAT* data. Various other sidebands corresponding to the first, second, and third harmonics of Ω_0 and $\Omega_{\rm pr}$ are also present in Figures 3 and 4. No significant power is seen, however, at the previously reported superhump period of 6.3 hr seen in optical photometry by Retter et al. (2003). The X-ray power level for this period has been shown with a vertical dotted line in Figure 3.

We also extracted a CLEANed power spectrum from the 1995 *ASCA* SIS0 observations of TV Col in the 0.7–10 keV energy band, using the same values for the number of CLEAN iterations and the loop gain as used for generating the *RXTE* and the *ROSAT* power spectra. The power spectrum shows a strong peak at a period of 1909.9 ± 9.5 s, consistent with the value of ω derived from the *RXTE* and the *ROSAT* data. A prominent peak is also observed at a period of $19{,}099 \pm 957$ s, consistent with the 5.5 hr binary period.

3.2. *Energy Dependence of Power Spectrum*

We have also studied the effect of different energy bands on the power spectrum and obtained power spectra for three different energy bands, viz., 2–5, 5–10, and 10–20 keV using the *RXTE* data, and two softer energy bands of 0.1–0.75 keV and 0.75–2.2 keV from the *ROSAT* data. These energy resolved CLEANed power spectra are displayed in Figures 5 and 6 for the *RXTE* and the *ROSAT* bands, respectively. The absolute power of the various identified frequency components in these energy resolved power spectra are listed in Table 2. The peak power corresponding to Ω_0 decreases with energy and is near the noise level in the highest energy band (see Fig. 5). However, some of the sideband frequencies for the orbital

TABLE 2
ABSOLUTE POWER OF VARIOUS COMPONENTS

FREQUENCY COMPONENT	PERIOD (s)	ABSOLUTE POWER (count s^{-1})^2						
		ROSAT ($\times 10^{-4}$)			*RXTE*			
		0.1–2.2 keV	0.1–0.75 keV	0.75–2.2 keV	2–20 keV	2–5 keV	5–10 keV	10–20 keV
Noise [a]	...	0.4000	0.1500	0.2300	0.01	0.0012	0.0032	0.0008
$\Omega_0 - 3\Omega_{pr}$	23909 ± 394	...	...	...	0.0989	...	0.0475	...
Ω_0	19819 ± 167	9.2758	2.4250	2.3702	0.4182	0.1805	0.0609	...
$\Omega_0 + \Omega_{pr}$	18727 ± 235	9.5462	2.6936	2.4249	...	0.0810	...	...
$2\Omega_0 - 3\Omega_{pr}$	10831 ± 79	...	...	...	0.2408	0.0456	0.0494	0.0038
$2\Omega_0 + \Omega_{pr}$	9624 ± 63	...	...	...	0.1562	0.0357	...	...
$2\Omega_0 + 3\Omega_{pr}$	9117 ± 173	4.3506	1.3509	1.5346	...	...	...	...
$3\Omega_0$	6600 ± 30	...	...	...	0.0927	0.0128	0.0325	0.0023
$3\Omega_0 + \Omega_{pr}$	6476 ± 30	...	...	...	0.1250	0.0341	0.0309	...
$4\Omega_0 - 3\Omega_{pr}$	5172 ± 18	...	...	...	0.0850	...	0.0118	0.0035
$4\Omega_0 - \Omega_{pr}$	5022 ± 53	1.1842	...	...	...	...	...	...
$4\Omega_0 + \Omega_{pr}$	4880 ± 16	...	...	...	0.0934	0.0285	...	...
ω	1909.67 ± 2.5	14.038	1.9979	5.3934	1.6336	0.2966	0.4650	0.0252
$\omega + \Omega_0$	1742 ± 2	...	0.3095	...	...	...	...	0.0023
$\omega + 2\Omega_0$	1601 ± 2	...	...	...	0.0322	...	...	0.0028
$\omega + 3\Omega_0$	1481 ± 1.5	...	...	...	0.0263	...	0.0108	0.0042
$2\omega + 3\Omega_0$	834 ± 0.5	...	0.6458	...	0.0943	0.0136	...	...
$3\omega - 2\Omega_0$	680 ± 1	1.1100	0.7363	...	...	...	...	...
Unidentified	8889 ± 54	...	...	...	...	...	...	0.0051
	7885 ± 42	...	...	...	...	...	...	0.0073
	7407 ± 37	...	...	...	0.1424	0.0218	0.0348	...
	3703 ± 9	...	...	...	...	...	...	0.0053
	3650 ± 27	3.3994	0.5926	0.9645	...	...	...	...
	3595 ± 9	...	...	...	0.1307	0.0126	0.0387	...
	2993 ± 6	...	...	...	0.0818	...	0.0345	0.0059
	2810 ± 5	...	...	...	...	...	...	0.0057
	2452 ± 4	...	...	...	...	...	...	0.0046
	2335 ± 4	...	...	...	0.0786	...	0.0341	0.0045
	2195 ± 3	...	...	...	...	...	...	0.0051
	1771 ± 2	...	...	...	0.1231	...	0.0425	0.0023
	1697 ± 6	3.7944	...	1.7409	...	...	...	...
	1264 ± 3	3.5933	...	2.1954	...	...	...	...
	800 ± 0.4	...	...	...	0.1642	0.0166	0.0433	0.0045
	758 ± 1	...	...	1.1718	...	...	...	...
	425 ± 0.4	...	...	1.1595	...	...	...	...

NOTES.—Absolute power of various components detected above the noise level at frequencies corresponding to the spin period (ω = 1909.67 s), orbital period (Ω_0 = 5.5 hr), and sideband frequencies from their combinations as predicted in a model by Norton et al. 1996. Sideband frequencies from the combination of orbital period and the 4 day precession period (Ω_{pr}), and strong but unidentified components are also listed along with their power.

[a] Absolute power for noise level with 90% confidence.

period seem to be present at higher energies, indicating that the effect of orbital modulation may still be present. On the other hand, the peak power for Ω_0 in the softest energy band of 0.1–0.75 keV becomes comparable with that for ω. According to the theoretical model of Norton et al. (1996), the amplitude at the frequency component $\omega + 3\Omega_0$ is predicted to be zero. We observed a power at this component that is above the noise level in the high energy bands (greater than 2 keV) but is not detected in the soft energy bands (less than 2 keV). We also observed a little power above the noise level corresponding to the second harmonic ($3\Omega_0$) of the orbital period above 2 keV energy bands.

As listed in Table 2, it is mostly the positive sideband frequencies due to the interaction of ω and Ω_0 that are present in the power spectra of TV Col, the corresponding negative sideband frequencies being absent. The only component present corresponding to the negative sideband frequency is $3\omega - 2\Omega_0$ in *ROSAT* soft X-ray energy bands. The energy resolved power spectra also shows the presence of several sideband frequency components due to Ω_0 and Ω_{pr} and their harmonics (Table 2).

3.3. *Spin Modulated Light Curves*

We have used the spin period derived by us using the 1996 *RXTE* data, since this is the most accurate determination so far, to fold all the data sets analyzed in this paper. The folded light curves in the three energy bands of *RXTE* are shown in the top three panels of Figure 7. The spin-folded light curve in the *ROSAT* soft X-ray energy band of 0.1–2.2 keV is shown in Figure 8 (*top*). Similarly, the spin-folded light curves for the *ASCA* energy bands of 0.7–2 keV and 2–10 keV are shown in the top two panels of Figure 9. Our attempts to obtain a new ephemeris for the spin period of TV Col were not successful since TV Col is a highly variable source and the shape profile of its spin-modulated light curve (see Figs. 1 and 2) changes from cycle to cycle making it very difficult to identify a permanent

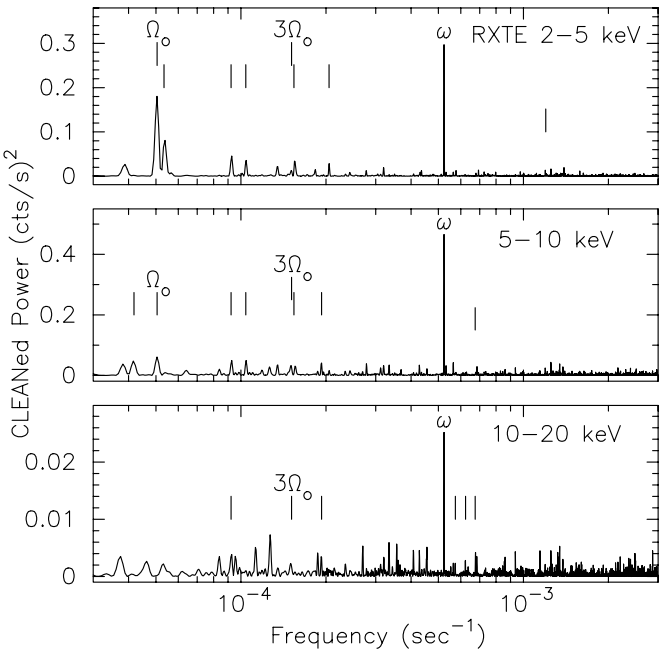

FIG. 5.—Energy-resolved CLEANed power spectra of TV Col in 2–5 keV, 5–10 keV, and 10–20 keV energy bands from the 1996 *RXTE* observations. See Table 2 for the corresponding tick mark frequency components.

feature with respect to which we can define the ephemeris. Therefore, an arbitrarily defined epoch, HJD = 2,450,304.5 was used here to fold all data with the spin period. The modulation is nearly sinusoidal in all the energy bands (see Figs. 7, 8, and 9) with the softer energy bands showing a relatively higher amplitude than the harder bands. The relative modulation amplitudes, defined as the ratio of the amplitude of the sine wave to the average intensity, are about 20% ± 2%, 14% ± 0.3%, 8.5% ± 0.2%, and 6% ± 0.5% of the mean intensity in the energy bands of 0.1–2.2 keV, 2–5 keV, 5–10 keV, and 10–20 keV, respectively. For the two *ASCA* energy bands of 0.7–2 keV and 2–10 keV, the modulation amplitudes are ∼17.5% ± 2.5% and 9% ± 2%, respectively. The modulation in the *ROSAT* band appears nearly out of phase by 180° compared with the hard *RXTE* bands which vary in phase with each other. However, the spin modulations in the *ASCA* energy bands of 0.7–2 keV and 2–10 keV are observed to be in phase with each other. The shape of the spin-folded light curve is also found to be energy-dependent (see Figs. 7, 8, and 9) thus confirming the previous results up to 10 keV by Norton & Watson (1989). The shape changes from a sinusoid to more like a flat-topped profile with increasing energy.

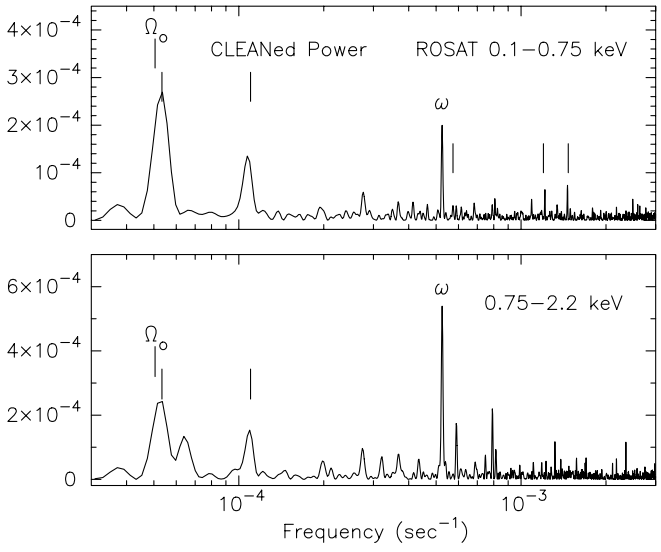

FIG. 6.—Energy-resolved CLEANed power spectra of TV Col in soft X-ray energy bands of 0.1–0.75 keV and 0.75–2.2 keV from the 1993 *ROSAT* observations. See Table 2 for the corresponding tick mark frequency components.

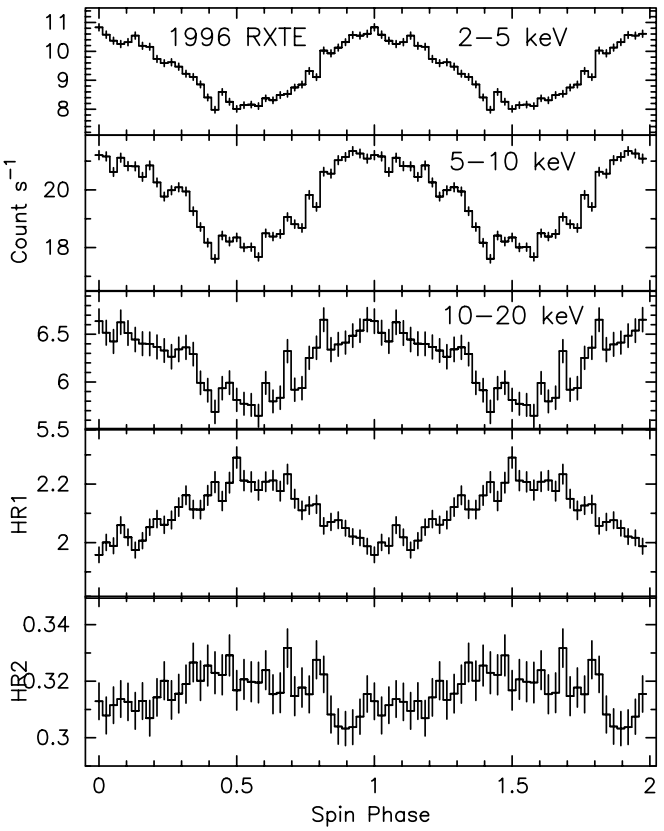

FIG. 7.—Light curves folded on the spin period derived using the 1996 *RXTE* data in 2–5 keV, 5–10 keV, and 10–20 keV energy bands (*top three panels*). Hardness ratio curves HR1 and HR2 folded using the same spin period are shown in the bottom two panels (for definitions of HR1 and HR2 please see the text). The bin time is 50 s throughout.

Hardness ratio curves obtained from the three energy bands of *RXTE* are shown plotted in the bottom two panels of the Figure 7 as a function of the spin phase. Two hardness ratios, HR1 and HR2, are defined for the *RXTE* data as follows: HR1 is the ratio of the count rate in 5–10 keV to count rate in 2–5 keV energy bands, and HR2 is the ratio of the count rate in 10–20 keV to count rate in 5–10 keV energy bands. A third hardness ratio, HR3, is defined as the ratio of the count rate in 0.75–2.2 keV energy band to the count rate in 0.1–0.75 keV energy band for the *ROSAT* data and is shown plotted in Figure 8 (*bottom*) as a function of the spin phase. The hardness ratio, HR4, for the *ASCA* energy bands is defined as the ratio of the count rate in 2–10 keV energy band to the count rate in 0.7–2 keV energy band and is shown plotted in Figure 9 (*bottom*). HR1 shows a strong modulation being 180° out of phase with the intensity modulation, i.e., the maximum in HR1 occurs at the lowest intensity (spin phase = 0.5). A similar variation can also be seen in the HR2 but is less modulated. Hardness ratio HR3 hardly shows any effect due to spin modulation and remains constant over the entire spin

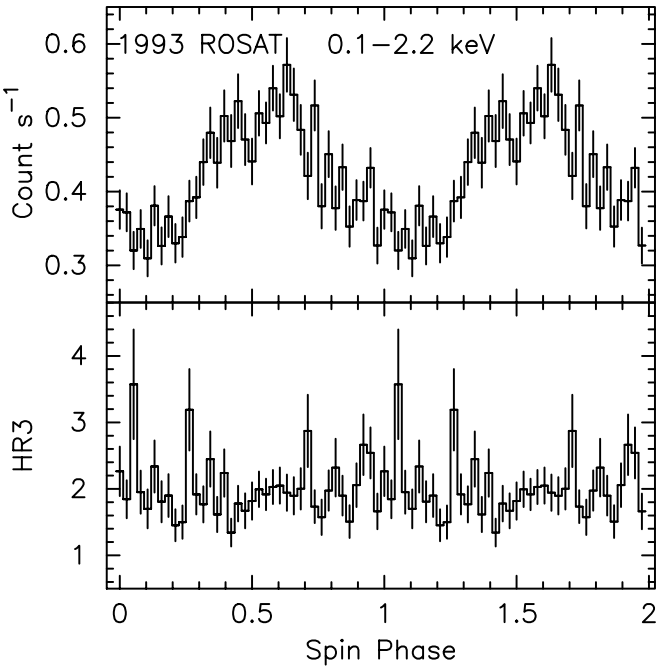

FIG. 8.—Spin phase folded light curve in soft X-ray energy band of 0.1–2.2 keV from the 1993 *ROSAT* observations (*top*). *Bottom*: The hardness ratio curve HR3 which is defined in text. The bin time is 50 s throughout.

cycle. The hardness ratio curve HR4 also does not show any significant variation over the entire spin cycle, except for a small change during the intensity minimum but with large error bars due to the low count rate in this phase range.

3.4. *Binary Period Modulated Light Curves*

We have used the most accurate ephemeris available for the orbital period as given by Augusteijn et al. (1994):

$$T(\mathrm{HJD}) = 2,447,151.2324(11) + 0.22859884(77)N$$

to fold data from all the three satellites. The folded light curves in four energy bands from soft (*ROSAT*) to hard (*RXTE*) energies are shown in Figure 10. Similar folded light curves for the *ASCA* energy bands are plotted in the top two panels of Figure 11. The effect of orbital modulation is seen as a large asymmetric dip, which is best seen in the 2–5 keV energy band. This dip is broad, spanning the phase range of 0.75–1.2 in the soft X-ray energy band. The main dip splits into two because of the presence of a small interpulse centered at phase 0.86. The two minima of these small dips occur at orbital phases of ∼0.80 and ∼0.93, respectively. The width of these low-intensity features appear to decrease with increasing energy—being the broadest in the *ROSAT* 0.1–2.2 keV soft X-ray band and visible at the highest energies only during the orbital phases of 0.75–1.0. Unfortunately, the data could not cover the complete orbital phase cycle during the 1993 *ROSAT* observations, and there is a data gap in the 0.8–0.9 phase range (see Fig. 10, *top*). This is, however, compensated by the *ASCA* observation in the 0.7–2 keV energy band that shows a clear dip during the 0.8–0.9 phase range. Persistent X-ray emission is seen during these low intensity phases.

Hardness ratios defined in § 3.3 have been plotted as a function of the orbital phase and shown in the bottom panels of Figure 11 (HR4) and in Figure 12 (HR1 to HR3). HR1 shows a strong increase during the minimum intensity (orbital phase = 0.7–1.0). The shape profile of this broad peak in HR1 is exactly opposite, but similar in size, to the broad dip seen in the folded light curve of Figure 10. A similar effect is also visible in the HR2. Hardness ratio HR3 also shows a small increase at phase 0.95 present in HR1 and HR2; however, the error bars are comparatively larger here because of the low count rate during intensity minimum in the *ROSAT* bands in this phase range. Hardness ratio HR4 also shows a strong increase during the minimum intensity phase and remains

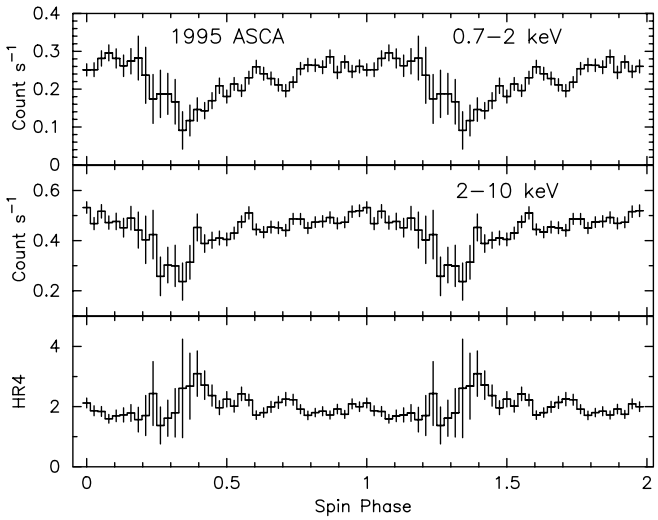

FIG. 9.—Spin phase folded X-ray light curves in two energy bands from the 1995 ASCA SIS0 observations (*top two panels*). Hardness ratio curve HR4, as defined in the text, is shown plotted in the bottom panel. The bin time is 50 s throughout.

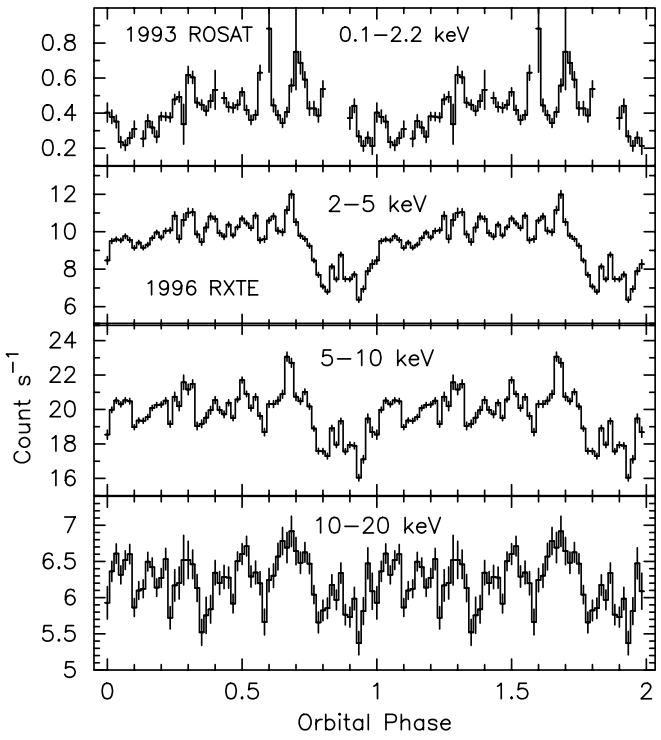

FIG. 10.—Light curves folded on the orbital period using the ephemeris as given by Augusteijn et al. (1994). *Top*: the *ROSAT* soft X-ray light curve in 0.1–2.2 keV energy band. The remaining three panels show *RXTE* hard X-ray light curves in 2–5 keV, 5–10 keV, and 10–20 keV energy bands, respectively. The bin time is 329 s throughout.

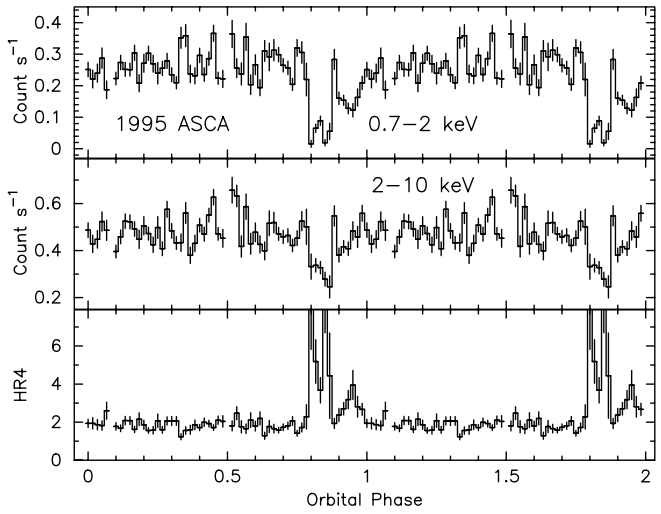

FIG. 11.—Light curves folded on the orbital period using the ephemeris as given by Augusteijn et al. (1994) from the 1995 ASCA SIS0 observations (*top two panels*). Hardness ratio HR4, as defined in the text, is shown plotted in the bottom panel. The bin time is 329 s throughout.

almost constant during the rest of the binary cycle. The error bars during the phase range 0.8–0.9 are very large here because of the small count rate in this phase range.

4. DISCUSSION

The longest ever observed X-ray light curves of TV Col in various energy bands ranging from the very soft (0.1 keV) to hard (20 keV) X-rays have been analyzed in detail. The light curves have the best timing resolution and the highest sensitivity at the highest energies reported so far. A variety of behavior and complexity is observed in these light curves. Power density spectra obtained using the CLEAN and the Bayesian methods show strong peaks at two fundamental periods, i.e., the spin period and the orbital period of the system in both the soft X-ray and the hard X-ray bands, indicating a strong modulation at these periods. In general, the X-ray modulation at the spin period can arise due to the occultation of the X-ray–emitting source by the white dwarf body and/or due to photoelectric absorption and electron scattering in the accretion curtain. On the other hand, the most common cause for the orbital modulation in X-ray light curves is due to attenuation of X-rays from material fixed in the orbital frame. The results presented in § 3 are examined and discussed below within the above framework.

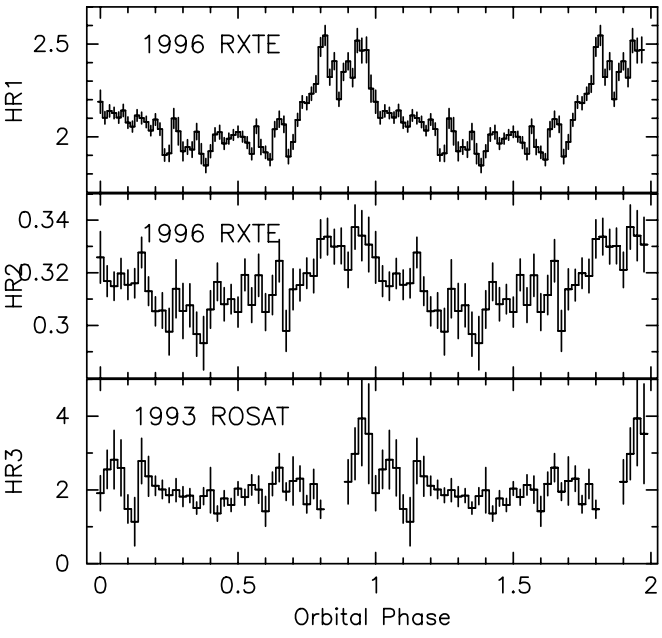

FIG. 12.—Hardness ratio curves folded on the orbital period using the ephemeris as given by Augusteijn et al. (1994). For definitions of hardness ratios HR1, HR2, and HR3, please see the text.

4.1. *Power Spectra*

Various frequency components corresponding to the interaction of three fundamental periods (spin, orbital, and precession) and sidebands due to their harmonics are present in the power density spectra of TV Col. Norton et al. (1996) have predicted various frequency components that can be present in a power spectrum of an IP assuming some generally known sites for emission and absorption components. The presence of several components in the power spectra of TV Col suggest contribution from several emission and attenuation sites that are listed by Norton et al. (1996). Frequency components in TV Col are better resolved in the 1996 *RXTE* data because of its better sampling and long length of observation compared with the 1993 *ROSAT* observation. Several of these components are merged with each other in the 1993 *ROSAT* data, especially at low frequencies, and so is the case with the 1995 *ASCA* data as well. Significant power at frequency components corresponding to ω, Ω_0, $\omega + \Omega_0$, $\omega + 2\Omega_0$, and $3\omega - 2\Omega_0$ in several energy bands, predict that TV Col is an asymmetric system in which both the emission poles are not diametrically opposite and have slightly different emission properties (see Norton et al. 1996). The amount of asymmetry depends on whether the signal corresponding to the rotation of the asymmetrically placed poles is strong or weak. The presence of an additional source of emission due to the impact of the accretion stream with the accretion disk or magnetosphere is also predicted. A strong signal at the orbital period below 10 keV energy clearly indicates an explicit orbital modulation that is most likely due to the attenuation introduced by the impact site (see below § 4.3). In addition, the influence of the 4 day precession period has been observed in term of its various sideband frequencies with the orbital period.

The absence of power corresponding to the frequency at the sideband $\omega - \Omega_0$ and presence of dominating power at ω suggest a significant contribution from the disk-fed accretion for TV Col. According to Wynn & King (1992), the power spectrum of an IP with a simple diskless geometry is dominated by signals at frequency components $\omega - \Omega_0$ or $2\omega - \Omega_0$. The absence of dominating power at these frequency components in TV Col suggests a predominant contribution from the disk-fed accretion component. It is, however, very unlikely that the accretion is taking place entirely via the disk because of the presence of various other sideband frequency components. Signal at $\omega + \Omega_0$ is seen in two energy bands (see Table 2), indicating amplitude modulation of the spin pulse at the orbital period and suggesting the influence of accretion by a stream. In addition, the presence of $3\omega - 2\Omega_0$ and the other sideband components as listed in Table 2 supports the stream-fed accretion for TV Col.

The power spectra of TV Col, thus, suggest a rather complex mode of accretion in which the white dwarf accretes via both the disk and the accretion stream. An asymmetry in the geometry of

the X-ray source is also implied. Similar power spectra with different positive and negative sideband frequencies corresponding to the spin and the orbital period are also observed in an IP TX Columbae by Norton et al. (1997), suggesting that TV Col may have a close resemblance with TX Col. However, unlike TX Col, we did not observe any change in the accretion mode for TV Col during the two epochs of observations.

4.2. *X-Ray Spin Modulation*

The spin modulation of the source is observed to be nearly sinusoidal and the amplitude of the modulation is found to decrease with increase in energy (Figs. 7, 8, and 9). The energy-dependent amplitudes have been measured more precisely here (see § 3.3) as compared with the previous measurements with the *EXOSAT* (Norton & Watson 1989). The average weighted values of modulation depth reported by Norton & Watson (1989) from three *EXOSAT* observations were $\sim 35\% \pm 22\%$, $31\% \pm 3\%$, $19\% \pm 3\%$, and $18\% \pm 6\%$ in the energy bands of 0.05–2.0 keV, 2–4 keV, 4–6 keV, and 6–10 keV, respectively. Norton & Watson (1989) defined the modulation depth as the peak-to-peak sinusoidal amplitude divided by the maximum flux, and the values reported here are consistent with their observations. They also indicated the possibility of spin modulation in soft X-ray band being 180° out of phase compared with the hard X-ray band, as has been observed here in the *ROSAT* and the *RXTE* data. However, the energy-resolved folded light curves obtained from *ASCA* vary in phase with each other (see § 3.3). The absence of any phase shift in the two spin-folded *ASCA* light curves, in the energy bands above and below 2 keV, suggests that the phase mismatch between the *ROSAT* and the *RXTE* light curves is most likely due to the lack of precision in the ephemeris for the spin period of the white dwarf in TV Col. Therefore, a precise measurement of the ephemeris for the spin of the white dwarf is required.

Energy dependence of the spin amplitude is one of the unique properties of IPs that is commonly observed in this subclass of magnetic CVs (e.g., in FO Aqr by Beardmore et al. 1998). The change in the shape of the X-ray light curves with energy, from a sinusoid in the soft X-rays to a near flat-top shape in the hard X-rays, suggests that the harder X-ray emission comes from a relatively larger region. Since the most probable site for hard X-ray emission is the shocked plasma in the postshock region in the accretion column, therefore it is quite possible that in this case the shocked plasma is at a considerable height above the white dwarf surface. The hardness ratios HR1 and HR2 from the 1996 *RXTE* data are spin-modulated but out of phase with the intensity variations. The anti-correlation between the intensity and the hardness ratio curves HR1 and HR2 observed in TV Col suggests that photoelectric absorption of X-rays above 2 keV could be responsible for the modulation. However, the lack of variation in the hardness ratio HR3 and a strong intensity modulation observed in the very soft band with the *ROSAT* suggest that the softest X-rays are coming from an unobscured region or that the absorbers responsible for variations above 2 keV do not cover the source completely. Below we test this hypothesis and try to estimate the amount of absorption and covering fractions required to produce the observed spin modulation in TV Col.

Broadband X-ray spectrum taken with *ROSAT* (averaged for the 1993 observation) and *RXTE* (averaged for the longest observation of 1996 August 13 with a similar modulation depth as the averaged data from all the 1996 observations) can be explained by a joint fit to a simple spectral model consisting of a partially but heavily absorbed thermal bremsstrahlung component, interstellar absorption in the line of sight, and a Gaussian line at 6.6 keV. The partial covering model was successfully employed by Norton & Watson (1989) to explain the *EXSOAT* data of IPs, including TV Col. If the bremsstrahlung continuum intensity is not constrained to be the same in the two observations separated by 3 yr, then the best-fit values for spectral parameters are as follows: covering fraction, $C_f = 0.94^{+0.01}_{-0.04}$; column density, $N_{\rm H} = 7.5^{+0.6}_{-0.4} \times 10^{22}$ cm^{-2}; thermal bremsstrahlung temperature, $kT = 23.5 \pm 1.2$ keV; and an interstellar absorption of $2.1^{+0.2}_{-0.1} \times 10^{20}$ cm^{-2} being consistent with other estimates in this direction. The minimum reduced χ^2 (χ^2_ν) for this best fit is 1.15 for 87 degrees of freedom (dof), and errors quoted are with 90% confidence. Constraining the bremsstrahlung continuum to be the same in the two observations gives the best fit with $\chi^2_\nu = 1.23$ for 88 dof, and the best-fit parameters in this case are $C_f = 0.84^{+0.01}_{-0.01}$, $N_{\rm H} = 9.6^{+0.3}_{-0.4} \times 10^{22}$ cm^{-2}, and $kT = 21.7^{+1.2}_{-1.0}$ keV, with the interstellar absorption being the same as before. In either case, keeping the values of the temperature and the Gaussian line emission parameters fixed at their best-fit values, we were able to reproduce the observed intensity and hardness ratio modulations by varying the $N_{\rm H}$ and C_f. The value of $N_{\rm H}$ had to be changed by 12%–19% from its best-fit value to reproduce the observed modulation in HR1 and HR2 and the count rates in the 2–5 keV, 5–10 keV, and 10–20 keV energy bands. As the $N_{\rm H}$ increases, HR1 and HR2 increase and the count rates above 2 keV fall without affecting HR3 or the counts below 2 keV. A small simultaneous decrease ($\sim$0.06) in the C_f is required to explain the simultaneous increase in the soft X-rays below 2 keV. A similar exercise was also carried out for the *ASCA* data using the same spectral model, as before. It was observed that a change in $N_{\rm H}$ ($5.0^{+0.8}_{-0.7} \times 10^{22}$ cm^{-2} for the averaged data) alone is not sufficient to reproduce the intensity modulation at energies below 2 keV, as was the case with the *ROSAT* data. In order to reproduce the intensity modulations in the two *ASCA* bands and the variations in HR4, we had to change the value of $N_{\rm H}$ by a factor of 2 accompanied by a simultaneous increase (15%) in C_f (0.69 ± 0.02 for the averaged data). In this case, the best-fit values for the $N_{\rm H}$ and C_f are much lower than the corresponding values obtained from the *ROSAT* and the *RXTE* joint fit. Even though the change in the values of $N_{\rm H}$ and C_f required to reproduce the amplitude modulation in *ASCA* data is comparatively larger, it should be noted, however, that the maximum values of $N_{\rm H}$ and C_f are comparable with the values required for the *ROSAT* and the *RXTE* data. These results suggest that a source partially covered with dense neutral material can successfully explain the observed modulation in intensity and the hardness ratio curve in the *ASCA* data also.

Therefore, it is quite possible to explain the observed spin-modulated intensity and the hardness ratio curves by invoking a dense partial absorber with varying hydrogen column density and a slightly varying covering fraction in the accretion channel. The real situation can be far more complex, however, with several ionized and cold absorbers in front of shocked plasma emission component as has been seen in higher spectral resolution data obtained with *ASCA* (Ezuka & Ishida 1999). Another possibility that the observed characteristics of the spin modulation are due to a change in the shape of X-ray beam with energy cannot be ruled out.

4.3. *X-Ray Orbital Modulation*

The orbital modulation reveals light curves that are much more structured and nonsinusoidal as compared with the

spin-modulated light curves. The hard X-ray (greater than 2 keV) intensity curves show a broad energy-dependent dip between $\phi = 0.75$–1.00. Such energy-dependent features modulated over orbital period are common in IPs (Hellier et al. 1993). Again in this case the energy-dependent nature of this dip and its anti-correlation with hardness ratio suggests that the photoelectric absorption is very likely the primary cause for its origin. The hardness ratios during this broad intensity dip are observed to increase significantly, thus indicating a strong absorption of X-rays. Material with a high column density fixed in the orbital frame is, therefore, required to cause these absorption effects. Repeating the exercise described in § 4.2 we found that increasing the value of $N_{\rm H}$ by 60%–65% from its best-fit value for the averaged data can reproduce the maximum values in HR1 and HR2 and the dip in the count rates above 2 keV in *RXTE* data. For the *ROSAT* soft X-ray band, the dip is the broadest (see Fig. 10) with a significant substructure, but the corresponding hardness ratio HR3 (Fig. 11) does not clearly show a significant variation, as seen in HR1 and HR2. There is, however, a data gap during this phase coverage followed by a small increase in HR3 during $\phi = 0.9$–1.0 accompanied by a decrease in intensity in the soft (less than 2 keV) X-ray band thus giving some indication about the contribution from absorption effect to produce the dip. The change in $N_{\rm H}$ invoked above for explaining the *RXTE* data in the dip is, however, not sufficient to account for a corresponding change in the soft X-ray intensity during the dip, unless it is accompanied by a small increase ($\sim$0.02) in C_f. Similar results are obtained from the *ASCA* data where increasing the value of $N_{\rm H}$ by $\sim$70% from its average value can reproduce the observed intensity minimum in the 2–10 keV band but is not sufficient to account for the intensity minimum in the 0.7–2 keV band. In order to reproduce the dip minimum in both the energy bands and the maximum in the hardness ratio, we have to simultaneously increase the value of C_f by 20%. These results confirm that a partially covered absorber(s) can produce the dip modulated with the orbital period. It is also very likely that the absorbing material is distributed nonhomogeneously because of the structured profile seen during the broad dip in the light curves and the hardness ratio curves (see Figs. 10, 11, and 12). According to a globally accepted view about orbital modulation in IPs, this absorbing material is most likely situated near the site where the accretion stream from the secondary impacts on to the accretion disk or the magnetosphere. If this is the case with TV Col, then the inclination of the system should be high enough for the material, splashed out due to the impact of accretion stream, to cross the line of sight and produce the absorption dip modulated over orbital period. This is consistent with the estimated value of $70^\circ \pm 3^\circ$ for the inclination angle of TV Col obtained using the observed length and depth of the eclipse from optical data (Hellier et al. 1991). The broad dip in the hard X-ray light curves splits into two small dips (Figs. 10 and 11) suggesting that there may be two impact sites. This again implies that the accretion stream is highly inhomogeneous.

Similar absorption dips at binary phase 0.7–0.8 were weakly hinted at in the *EXOSAT* observations reported by Hellier et al. (1993). The absorption dips observed here with the *RXTE* (and the *ASCA*) are clear, unambiguous, and can be seen in all the orbital cycles covered by the observations. Such absorption dips have also been observed in several other IPs and are similar to those seen in the low-mass X-ray binaries (LMXBs) (Hellier et al. 1993). The likely cause for these dips in LMXBs is considered to be absorbing material above the plane of the accretion disk. In IPs where the stream accretion is also present the impact of the stream with the magnetosphere could produce shocks and throw some material out of the plane of the accretion disk.

The light curve folded on the orbital period in the highest energy band of 10–20 keV shows a negligible dip in intensity as compared with the folded light curves in the other energy bands. This suggests that the hard (10–20 keV) X-ray emission is almost unaffected by the orbital motions of the secondary star, consistent with the interpretation for dips at lower energies invoking absorbers.

5. CONCLUSIONS

Analysis of the longest hard and soft X-ray observations of TV Col with the *RXTE*, *ROSAT* and *ASCA* satellites leads us to the following conclusions:

1. Power density spectra of X-ray emission from TV Col show strong peaks at frequencies ω and Ω_0 suggesting these to be two fundamental frequencies of the system, i.e., the spin frequency and the orbital frequency. The presence of spin modulation in X-rays is thus confirmed and a significant power at ω is detected at all energies between 0.1 to 20 keV. The Ω_0 component is clearly present in the energy bands below 10 keV but is absent in the hardest energy band of 10–20 keV.

2. Significant power at two fundamental periods ω and Ω_0 and several sideband components of these two periods in the power spectra of TV Col provides evidence that contributions from both the disk-fed and the stream-fed accretion are present. The presence of certain sidebands of ω suggests asymmetrically placed poles. The effects of 4 day precession period can also be seen in the sidebands of Ω_0.

3. Modulation at the spin period being a function of energy is confirmed. It is $\sim$3–4 times larger in the softest X-rays when compared with the value in the hardest X-rays observed. The observed energy-dependent spin modulation and its anti-correlation with the hardness ratios defined above 2 keV can be explained by a partially covered absorber system, with a small change in the covering fraction being sufficient to explain the in-phase soft X-ray modulation without affecting the X-ray intensity above 2 keV.

4. The effect of the orbital period is seen clearly in the hard and soft X-ray light curves of TV Col. Modulation due to the orbital period is also seen to be more prominent in the soft X-rays than in the hard X-rays. X-ray light curves show a broad dip at orbital phase between $\phi = 0.7$–1.0. The hardness ratio variations during the dip can be understood by invoking an additional absorber (or absorbers) co-rotating in the orbital frame. A significant substructure during the dip suggests that these additional absorbers may be inhomogeneous. The absorbers could be located near the region where the accretion stream interacts with the accretion disk.

This research has made use of data obtained from the High Energy Astrophysics Science Archive Research Center (HEASARC), provided by NASA's Goddard Space Flight Center. V. R. R. is pleased to acknowledge partial support from the Kanwal Rekhi Scholarship of the TIFR Endowment Fund. We thank an anonymous referee for useful comments and suggestions. Starlink is funded by PPARC and based at the Rutherford Appleton Laboratory, which is part of Council for

the Central Laboratory of the Research Councils, UK. The research of E. M. S. was supported by contract number NAS 8-39073 to SAO. The research of P. E. B. was supported by contract number NAG 5-10247 to STScI.

REFERENCES

Augusteijn, T., Heemskerk, M. H. M., Zwarthoed, G. A. A., & van Paradijs, J. 1994, A&AS, 107, 219
Barrett, P., O'Donoghue, D., & Warner, B. 1988, MNRAS, 233, 759
Beardmore, A. P., Mukai, K., Norton, A. J., Osborne, J. P., & Hellier, C. 1998, MNRAS, 297, 337
Bonnet-Bidaud, J. M., Motch, C., & Mouchet, M. 1985, A&A, 143, 313
Bretthorst, G. L. 1988, Bayesian Spectrum Analysis and Parameter Estimation (New York: Springer-Verlag)
Charles, P. A., Thorstensen, J., Bowyer, S., & Middleditch, J. 1979, ApJ, 231, L131
Cooke, B. A., et al. 1978, MNRAS, 182, 489
Ezuka, H., & Ishida, M. 1999, ApJS, 120, 277
Gregory, P. C., & Loredo, T. J. 1996, ApJ, 473, 1059
Hellier, C. 1993, MNRAS, 264, 132
Hellier, C., Garlick, M. A., & Mason, K. O. 1993, MNRAS, 260, 299
Hellier, C., Mason, K. O., & Mittaz, J. P. D. 1991, MNRAS, 248, 5P
Hutchings, J. B., Crampton, D., Cowley, A. P., Thorstensen, J. R., & Charles, P. A. 1981, ApJ, 249, 680
Ishida, M., & Fujimoto, R. 1995, in Cataclysmic Variables, ed. A. Bianchini, M. Della Valle, & M. Orio (Dordrecht: Kluwer), 93
Jahoda, K., Swank, J. H., Giles, A. B., Stark, M. J., Strohmayer, T., Zhang, W., & Morgan, E. H. 1996, Proc. SPIE, 2808, 59
Mateo, M., Szkody, P., & Hutchings, J. 1985, ApJ, 288, 292
McArthur, B. E., et al. 2001, ApJ, 560, 907
Motch, C. 1981, A&A, 100, 277
Norton, A. J., Beardmore, A. P., & Taylor, P. 1996, MNRAS, 280, 937
Norton, A. J., Hellier, C., Beardmore, A. P., Wheatley, P. J., Osborne, J. P., & Taylor, P. 1997, MNRAS, 289, 362
Norton, A. J., McHardy, I. M., Lehto, H. J., & Watson, M. G. 1992a, MNRAS, 258, 697
Norton, A. J., & Watson, M. G. 1989, MNRAS, 237, 853
Norton, A. J., Watson, M. G., King, A. R., Lehto, H. J., & McHardy, I. M. 1992b, MNRAS, 254, 705
O'Donoghue, D. 2000, NewA Rev., 44, 45
Patterson, J. 2001, PASP, 113, 736
Retter, A., Hellier, C., Augusteijn, T., Naylor, T., Bedding, T. R., Bembrick, C., McCormick, J., & Velthuis, F. 2003, MNRAS, 340, 679
Roberts, D. H., Lehar, J., & Dreher, J. W. 1987, AJ, 93, 968
Schrijver, J., Brinkman, A. C., & van der Woerd, H. 1987, Ap&SS, 130, 261
Schrijver, J., Brinkman, A. C., van der Woerd, H., Watson, M. G., King, A. R., van Paradigs, J., & van der Klis, M. 1985, Space Sci. Rev., 40, 121
Singh, K. P., Rana, V. R., Mukerjee, K., Barrett, P., & Schlegel, E. M. 2003, in ASP Conf. Ser., Magnetic Cataclysmic Variables, ed. M. Cropper & S. Vrielmann (IAU Colloq. 190) (San Francisco: ASP), in press
Trümper, J. 1983, Adv. Space Res., 2, 241
Vrtilek, S. D., Silber, A., Primini, F., & Raymond, J. C. 1996, ApJ, 465, 951
Wynn, G. A., & King, A. R. 1992, MNRAS, 255, 83
Yamashita, A., et al. 1997, IEEE Trans. Nucl. Sci., 44, 847